



**Fermi National Accelerator Laboratory**

**FERMILAB-Conf-96/160-E**

**CDF**

**Branching Fractions of  $B^+ \rightarrow \psi(2S)K^+$  and  
 $B^0 \rightarrow \psi(2S)K^{*0}$  Decays at CDF**

Andreas Warburton

For the CDF Collaboration

*Fermi National Accelerator Laboratory  
P.O. Box 500, Batavia, Illinois 60510*

*University of Toronto  
Toronto, Ontario, Canada M5S1A7*

July 1996

Contributed Paper to the *28th International Conference on High Energy Physics (ICHEP96)*,  
Warsaw, Poland, July 25-31, 1996

## **Disclaimer**

*This report was prepared as an account of work sponsored by an agency of the United States Government. Neither the United States Government nor any agency thereof, nor any of their employees, makes any warranty, expressed or implied, or assumes any legal liability or responsibility for the accuracy, completeness, or usefulness of any information, apparatus, product, or process disclosed, or represents that its use would not infringe privately owned rights. Reference herein to any specific commercial product, process, or service by trade name, trademark, manufacturer, or otherwise, does not necessarily constitute or imply its endorsement, recommendation, or favoring by the United States Government or any agency thereof. The views and opinions of authors expressed herein do not necessarily state or reflect those of the United States Government or any agency thereof.*

# Branching Fractions of $B^+ \rightarrow \psi(2S)K^+$ and $B^0 \rightarrow \psi(2S)K^{*0}$ Decays at CDF<sup>1</sup>

The CDF Collaboration

## Abstract

This paper describes the observation of the decays  $B^+ \rightarrow \psi(2S)K^+$  and  $B^0 \rightarrow \psi(2S)K^{*(892)^0}$  in 1.8 TeV  $p\bar{p}$  collisions and presents measurements of the branching fractions  $\mathcal{B}(B^+ \rightarrow \psi(2S)K^+)$  and  $\mathcal{B}(B^0 \rightarrow \psi(2S)K^{*(892)^0})$  relative to  $\mathcal{B}(B^+ \rightarrow J/\psi K^+)$  and  $\mathcal{B}(B^0 \rightarrow J/\psi K^{*(892)^0})$ , respectively. The  $\psi(2S)$  mesons are reconstructed in both the  $\psi(2S) \rightarrow \mu^+\mu^-$  and  $\psi(2S) \rightarrow J/\psi\pi^+\pi^-$  channels. The world average branching fractions for the  $J/\psi$  channels are used to extract the absolute branching fractions  $\mathcal{B}(B^+ \rightarrow \psi(2S)K^+) = (6.8 \pm 1.0(\text{stat.}) \pm 1.4(\text{syst.})) \times 10^{-4}$  and  $\mathcal{B}(B^0 \rightarrow \psi(2S)K^{*(892)^0}) = (9.0 \pm 2.1(\text{stat.}) \pm 2.0(\text{syst.})) \times 10^{-4}$ .

## 1 Introduction

Decays of  $B$  mesons into  $J/\psi$  mesons have been the subject of much study at the Collider Detector at Fermilab (CDF) and at other experiments. Our 110 pb<sup>-1</sup> sample of  $\sqrt{s} = 1.8$  TeV  $p\bar{p}$  Tevatron collider data, however, enables us to investigate the lower-rate decays of  $B$  mesons into  $\psi(2S)$  final states. The radially excited  $\psi(2S)$  mesons, as in the case of the  $J/\psi$  mesons, decay into a pair of muons; however,  $\psi(2S)$  mesons can also decay through the mode  $\psi(2S) \rightarrow J/\psi\pi^+\pi^-$ .

---

<sup>1</sup>Contributed paper to the XXVIII International Conference on High Energy Physics, 25-31 July 1996, Warsaw, Poland.

In this analysis, we present evidence for the observation of the decays<sup>2</sup>  $B^+ \rightarrow \psi(2S)K^+$  and  $B^0 \rightarrow \psi(2S)K^{*0}$  in both the dimuon ( $\psi(2S) \rightarrow \mu^+\mu^-$ ) and hadronic cascade ( $\psi(2S) \rightarrow J/\psi\pi^+\pi^-$ ) channels. The relatively well-observed decays  $B^+ \rightarrow J/\psi K^+$  and  $B^0 \rightarrow J/\psi K^{*0}$  are investigated to both affirm the analysis technique and to permit the cancellation of several quantities when these modes are combined in a ratio with their  $\psi(2S)$  analogues. These ratios are also the subject of theoretical interest[2], since they facilitate the cancellation of some theoretical uncertainties and can be used to probe amplitude factorization hypotheses. Figures 1 and 2 depict the decays under study.

We measure the ratios of branching fractions  $\frac{\mathcal{B}(B^+ \rightarrow \psi(2S)K^+)}{\mathcal{B}(B^+ \rightarrow J/\psi K^+)}$  and  $\frac{\mathcal{B}(B^0 \rightarrow \psi(2S)K^{*0})}{\mathcal{B}(B^0 \rightarrow J/\psi K^{*0})}$ , and combine these ratios with the world average values for  $\mathcal{B}(B^+ \rightarrow J/\psi K^+)$  and  $\mathcal{B}(B^0 \rightarrow J/\psi K^{*0})$  to derive the absolute branching fractions  $\mathcal{B}(B^+ \rightarrow \psi(2S)K^+)$  and  $\mathcal{B}(B^0 \rightarrow \psi(2S)K^{*0})$ , respectively. We compare the results with limits and measurements from other experiments.

## 2 The CDF Detector

CDF is a multi-purpose detector designed to study  $p\bar{p}$  collisions produced by the Fermilab Tevatron collider. The interaction point is surrounded by three charged particle tracking detectors immersed in a 1.4 T solenoidal magnetic field. The tracking systems are enclosed within a hermetic calorimeter system, outside of which are located other charged particle detectors to identify muon candidates.

The innermost tracking device is a four-layer silicon-microstrip vertex detector (SVX) located in the region between 3.0 and 7.9 cm in radius from the beam axis[3]. The SVX, which allows for measurements in the  $r$ - $\varphi$  plane, is followed by a set of time projection chambers that measure charged particle trajectories out to a radius of 22 cm. An 84-layer drift chamber (CTC) measures three dimensional charged particle trajectories in the region between 30 and 130 cm in radius from the beam.

The muon detection system consists of 4-layer planar drift chambers separated from the interaction point by 5 to 8 interaction lengths of material. The muon system is capable of detecting muons with transverse momentum  $P_T \gtrsim 1.4$  GeV/ $c$  in a pseudorapidity interval  $|\eta| < 1.0$ . These and other components of the CDF detector are described in greater detail elsewhere[4].

---

<sup>2</sup>References to specific charge states imply the additional charge-conjugate state, and we use the notation  $K^{*0}$  in lieu of the standard[1],  $K^*(892)^0$ .

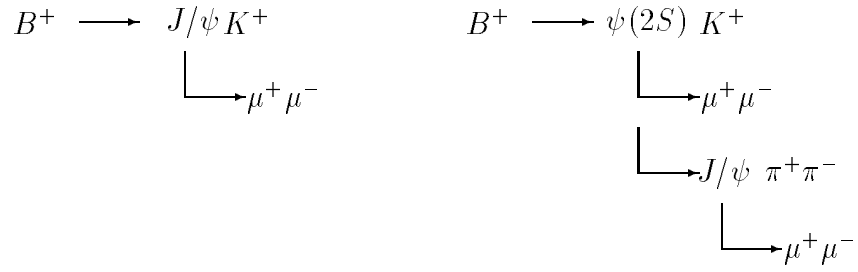


Figure 1: Schematic of the  $B^+$  decay modes.

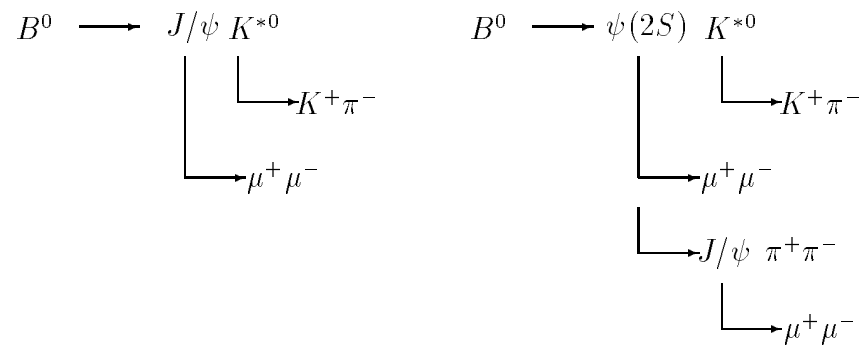


Figure 2: Schematic of the  $B^0$  decay modes.

### 3 Event Selection

Reconstruction of the exclusive decays in this analysis began with the identification of collisions containing two muon candidates. This was achieved by a three-level trigger system in which the first level trigger required that there be two track candidates observed in the muon system, the second level trigger required that associated charged tracks be detected in the CTC by partially reconstructing all charged tracks with a transverse momentum exceeding  $\sim 2.5$  GeV/ $c$ , and the third level trigger reconstructed the two CTC tracks, requiring that they match with two tracks in the muon chambers and that the dimuon invariant mass be between 2.7 and 4.1 GeV/ $c^2$ , a region where the dimuonic  $J/\psi$  and  $\psi(2S)$  resonances are expected to lie.

All candidate tracks in the analysis were required to have at least 4 hits in at least 2 of the 5 axial CTC superlayers and at least 2 hits in at least 2 of the 4 stereo CTC superlayers. Candidate tracks were required to possess  $P_T > 400$  MeV/ $c$  and intersect the endplate plane of the CTC at  $r > 132.0$  cm, which corresponds to the radius of the outermost CTC sense wire.

The two candidate charmonium muons were required to have charges of opposite sign and their CTC tracks, when extrapolated to the muon chambers, were required to match, within 3 standard deviations of the extrapolation and measurement uncertainties, a segment in the muon chambers, both in the transverse ( $r$ - $\varphi$ ) and longitudinal (beam axis) directions. A least-squares fit was performed on the two muon candidate tracks, constraining the two tracks to originate from a common point (vertex constraint). The probability of the fit ( $CL(\chi^2)$ ) was required to be greater than 0.01. The fit was repeated with the additional requirement that the dimuon invariant mass equal the world average[1]  $J/\psi$  or  $\psi(2S)$  mass (vertex+mass constraint), and the  $CL(\chi^2)$  of the fit was again required to be greater than 0.01. A  $P_T(\mu^+) > 2.5$  GeV/ $c$  requirement was imposed when reconstructing the  $B^0 \rightarrow \psi(2S)K^{*0}$ ;  $\psi(2S) \rightarrow \mu^+\mu^-$  channel and its companion  $J/\psi$  analogue. Such a cut was necessitated by the large background under the inclusive  $\psi(2S) \rightarrow \mu^+\mu^-$  resonance.

In the case of  $\psi(2S) \rightarrow J/\psi\pi^+\pi^-$  reconstruction, all four legs were required to originate from a common vertex and the 4-track invariant mass was constrained to equal the world average[1]  $\psi(2S)$  mass. Here again the fit probability was required to exceed 0.01. A Monte Carlo calculation of the dipion invariant mass distribution, which employed a phenomenological prescription for the  $\psi(2S) \rightarrow J/\psi\pi^+\pi^-$  matrix element[5], was compared with data in search of an efficient dipion selection criterion with a useful degree of background rejection.

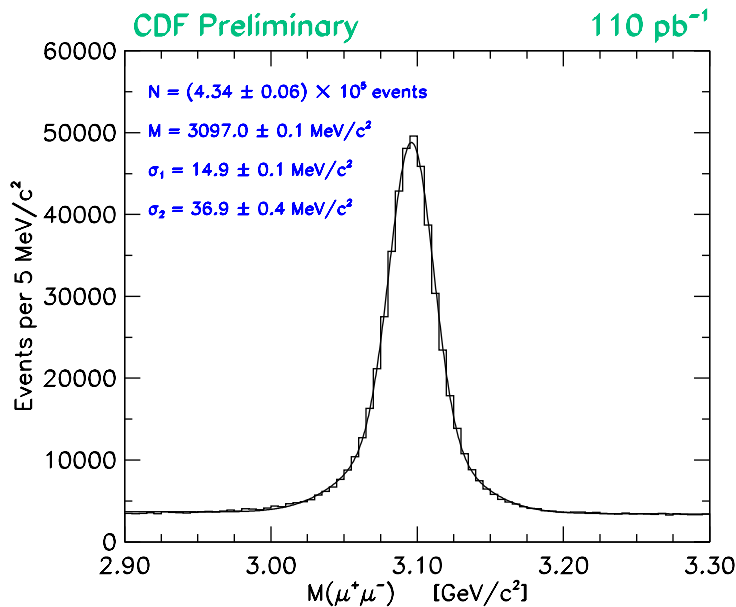


Figure 3: The  $J/\psi$  dimuon invariant mass distribution after a vertex constraint cut is applied. The fit is to a double Gaussian signal with linear amplitude and a linear background.

Consequently, the pre-constrained dipion invariant mass was required to lie in the range  $0.35 < M(\pi^+\pi^-) < 0.61 \text{ GeV}/c^2$ .

Plots of the inclusive charmonium invariant mass distributions, without the mass constraint requirement, for the  $J/\psi \rightarrow \mu^+\mu^-$ ,  $\psi(2S) \rightarrow \mu^+\mu^-$ , and  $\psi(2S) \rightarrow J/\psi\pi^+\pi^-$  reconstructions are presented in Figures 3, 4, and 5, respectively.

The exclusive  $B$  meson decay modes were reconstructed by forming charged particle combinations with the charmonium meson candidates. For the reconstruction of those channels with a  $K^+$  meson in the final state, every charged particle possessing  $P_T > 1.5 \text{ GeV}/c$  was initially considered to be a  $K^+$  candidate. For the reconstruction of those channels with a  $K^{*0}$  meson in the final state, all oppositely-charged track pairs with a combined  $P_T > 2.0 \text{ GeV}/c$  and a  $K^+\pi^-$  candidate invariant mass within  $0.08 \text{ GeV}/c^2$  of the world average  $K^*(892)^0$  mass[1] were initially considered to be  $K^{*0}$  candidates.

Depending on the mode of exclusive  $B$  meson decay being reconstructed, the track parameters for combinations of charmonium and  $K^+$  or  $K^{*0}$  candidates were fit with the requirement that all the charged tracks originate from a common decay point; moreover, the charmonium invariant mass was simultaneously constrained to its appropriate world average value[1], and the flight path of the  $B$  candidate was forced to lie parallel to its momentum vector in the transverse plane. The confidence level of this global fit had to be greater than

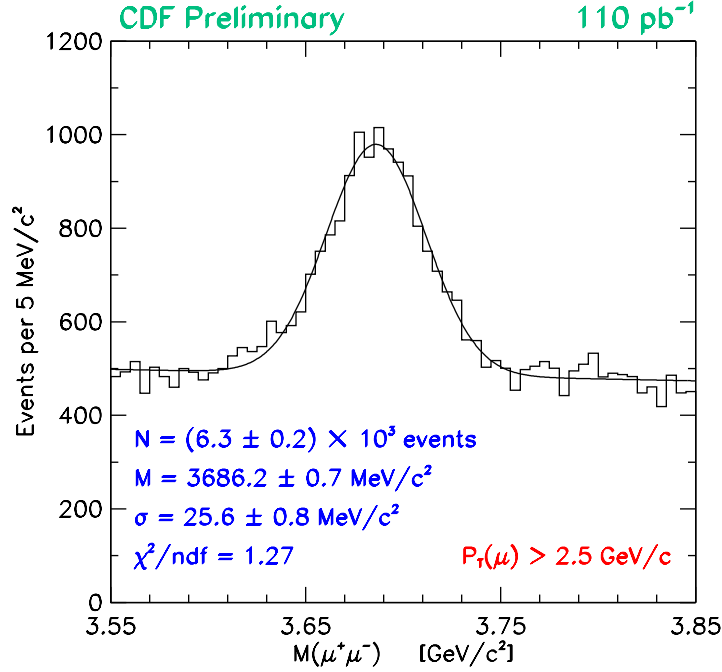


Figure 4: The  $\psi(2S)$  dimuon invariant mass distribution after a vertex constraint cut is applied. The fit is to a Gaussian signal and a linear background and there is a requirement that  $P_T(\mu^+) > 2.5 \text{ GeV}/c$ .

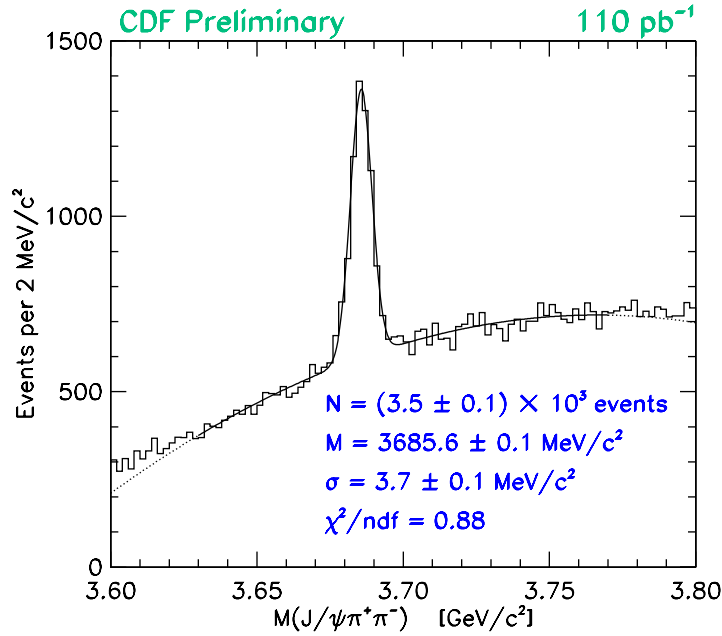


Figure 5: The  $J/\psi\pi^+\pi^-$  invariant mass distribution after a vertex constraint cut is applied to the two pion candidates. The fit is to a Gaussian signal and a cubic polynomial background.

0.01, and the proper decay length of the  $B$  meson candidate,  $c\tau$ , was required to exceed  $100 \mu\text{m}$ . Additional background rejection was achieved with the imposition of a momentum isolation cut,  $PBFAC > 0.55$ , on each  $B$  meson candidate. Here  $PBFAC$  is defined as  $PBFAC \equiv \frac{|\vec{P}(B)|}{|\vec{P}(B)| + \sum_{\# \text{ tracks}}^{R \leq 1.0} \vec{P} \cdot \frac{\vec{P}(B)}{|\vec{P}(B)|}}$ , with  $R \equiv \sqrt{(\Delta\eta)^2 + (\Delta\varphi)^2}$ . Finally, transverse momentum selection criteria  $P_T(B^+) > 6.0 \text{ GeV}/c$  and  $P_T(B^0) > 8.0 \text{ GeV}/c$  were placed on the charged and neutral  $B$  candidates, respectively.

## 4 Observed Candidate $B$ Meson Invariant Mass Distributions

The observed invariant mass distributions for the decays  $B^+ \rightarrow J/\psi K^+$ ,  $B^+ \rightarrow \psi(2S)K^+$ ;  $\psi(2S) \rightarrow \mu^+\mu^-$ , and  $B^+ \rightarrow \psi(2S)K^+$ ;  $\psi(2S) \rightarrow J/\psi\pi^+\pi^-$  are shown in Figures 6, 7, and 8, respectively. The signal widths in Figures 7 and 8 have been fixed to values predicted using Monte Carlo calculations. The predicted widths were calibrated with a scale factor determined by comparing the observed width of the  $B^+ \rightarrow J/\psi K^+$  decay in data to that predicted by the Monte Carlo calculation. This calibration factor was verified by also comparing the observed width of the  $J/\psi \rightarrow \mu^+\mu^-$  decay in data to that predicted by the Monte Carlo calculation. The event yields, which were calculated by performing binned log likelihood fits to the invariant mass distributions, are summarized in Table 1.

The observed invariant mass distributions for the decays  $B^0 \rightarrow J/\psi K^{*0}$ ,  $B^0 \rightarrow \psi(2S)K^{*0}$ ;  $\psi(2S) \rightarrow \mu^+\mu^-$ , and  $B^0 \rightarrow \psi(2S)K^{*0}$ ;  $\psi(2S) \rightarrow J/\psi\pi^+\pi^-$  are pictured in Figures 9, 11, and 12, respectively. Figure 10 also represents the decay  $B^0 \rightarrow J/\psi K^{*0}$ , but with the same cuts as used in the preparation of Figure 11 ( $P_T(\mu^+) > 2.5 \text{ GeV}/c$ ). The event yields are summarized in Table 1.

## 5 Summary of the Efficiencies

An advantage of measuring a ratio of branching fractions is that several effects divide out. This is the case for the tracking efficiency in the ratios involving the dimuon  $\psi(2S)$  decays; however, the ratios involving the hadronic cascade decay of the  $\psi(2S)$  have the topological distinction of two extra tracks that need to be reconstructed. We use a single track efficiency of  $(96.0 \pm 2.8)\%$  to correct for this effect in the  $B$  decays involving the  $\psi(2S) \rightarrow J/\psi\pi^+\pi^-$  channel.

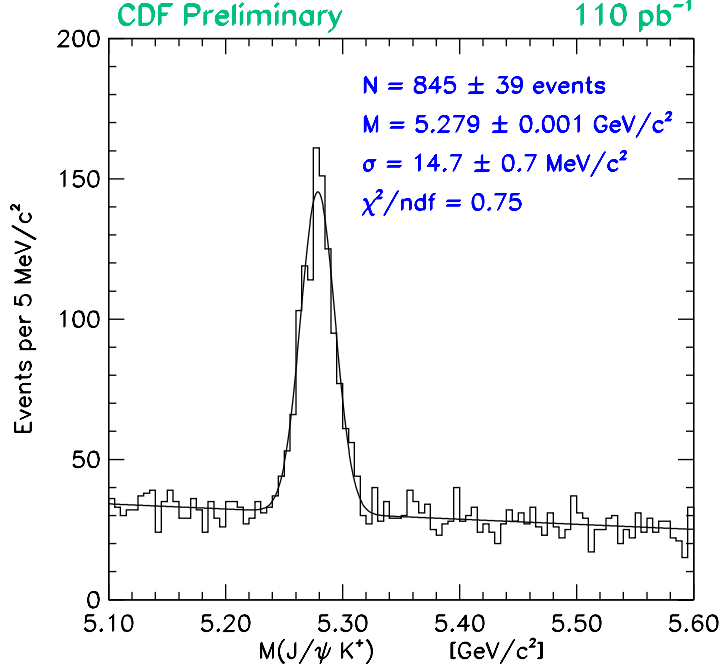


Figure 6: The  $J/\psi K^+$  invariant mass distribution. The fit is to a Gaussian signal and a linear background.

Decay Mode	Event Yield
$B^+ \rightarrow J/\psi K^+$	$845 \pm 39$
$B^+ \rightarrow \psi(2S)K^+; \psi(2S) \rightarrow \mu^+\mu^-$	$82.5 \pm 13.5$
$B^+ \rightarrow \psi(2S)K^+; \psi(2S) \rightarrow J/\psi \pi^+\pi^-$	$34.5 \pm 7.3$
$B^0 \rightarrow J/\psi K^{*0}$	$271 \pm 20$
$B^0 \rightarrow \psi(2S)K^{*0}; \psi(2S) \rightarrow \mu^+\mu^-$	$22.9 \pm 8.0$
$B^0 \rightarrow J/\psi K^{*0}$	$401 \pm 25$
$B^0 \rightarrow \psi(2S)K^{*0}; \psi(2S) \rightarrow J/\psi \pi^+\pi^-$	$24.7 \pm 6.9$

Table 1: Summary of event yields for 5 MeV/ $c^2$  binned likelihood fits. The grouping of the  $K^{*0}$  modes is on the basis of common selection criteria.

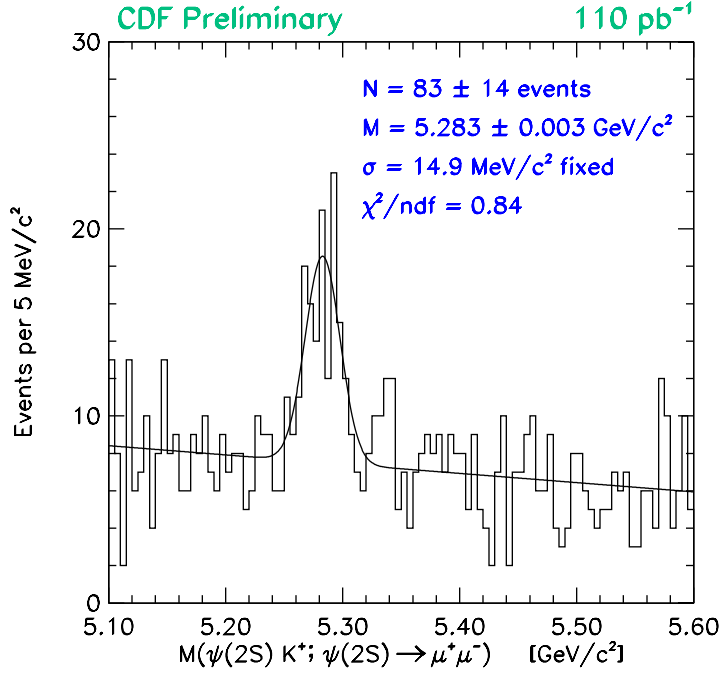


Figure 7: The  $\psi(2S)K^+; \psi(2S) \rightarrow \mu^+\mu^-$  invariant mass distribution. The fit is to a Gaussian signal and a linear background.

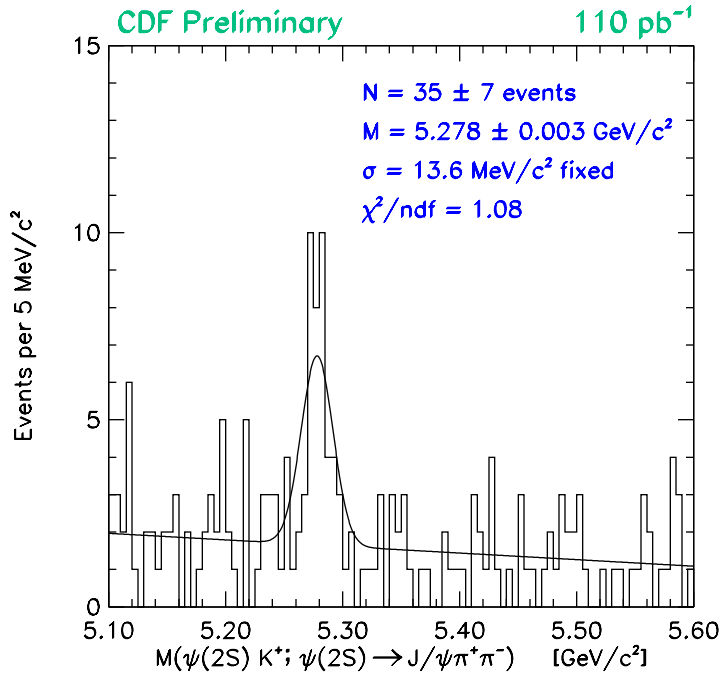


Figure 8: The  $\psi(2S)K^+; \psi(2S) \rightarrow J/\psi\pi^+\pi^-$  invariant mass distribution. The fit is to a Gaussian signal and a linear background.

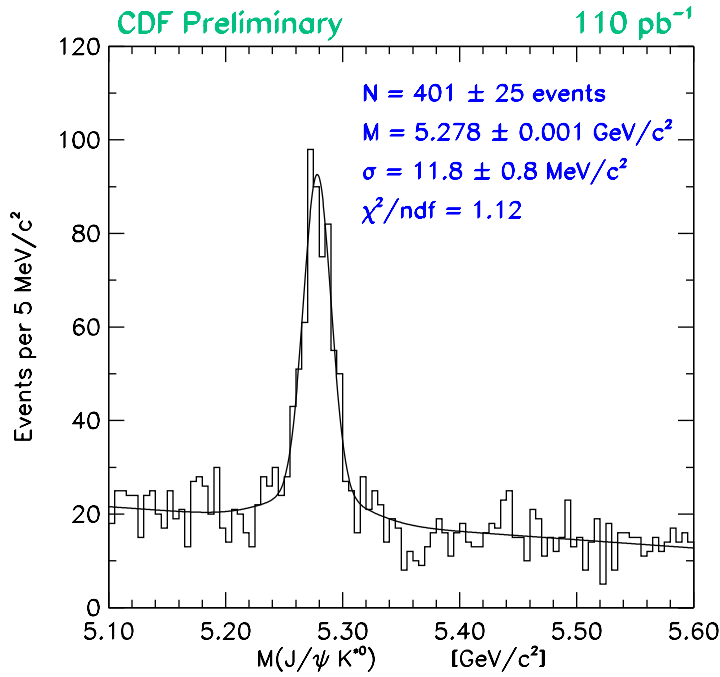


Figure 9: The  $J/\psi K^{*0}$  invariant mass distribution using the default event selection criteria. The fit is to a double Gaussian signal and a linear background. The first three fit parameters shown describe the Gaussian distribution of the correct  $K$ - $\pi$  combinations.

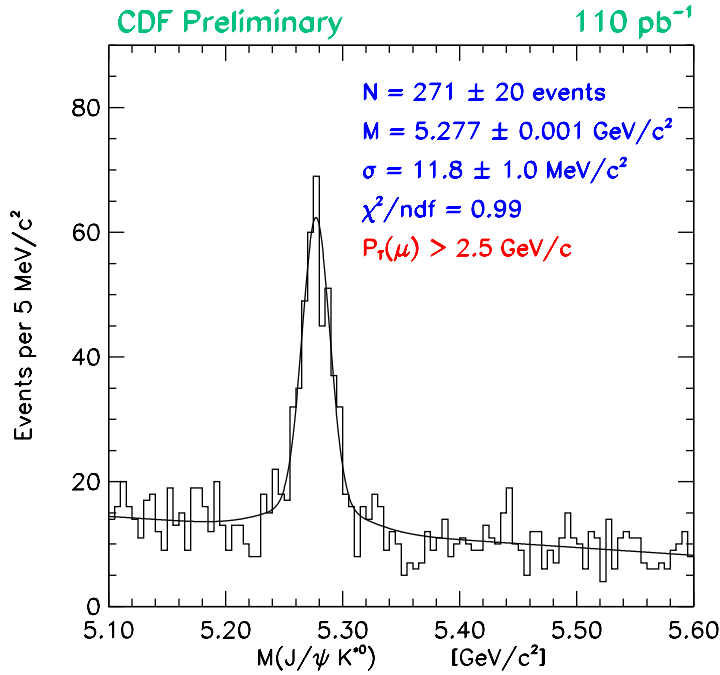


Figure 10: The  $J/\psi K^{*0}$  invariant mass distribution using the  $P_T(\mu^+) > 2.5 \text{ GeV}/c$  requirement. The fit is to a double Gaussian signal and a linear background. The first three fit parameters shown describe the Gaussian distribution of the correct  $K$ - $\pi$  combinations.

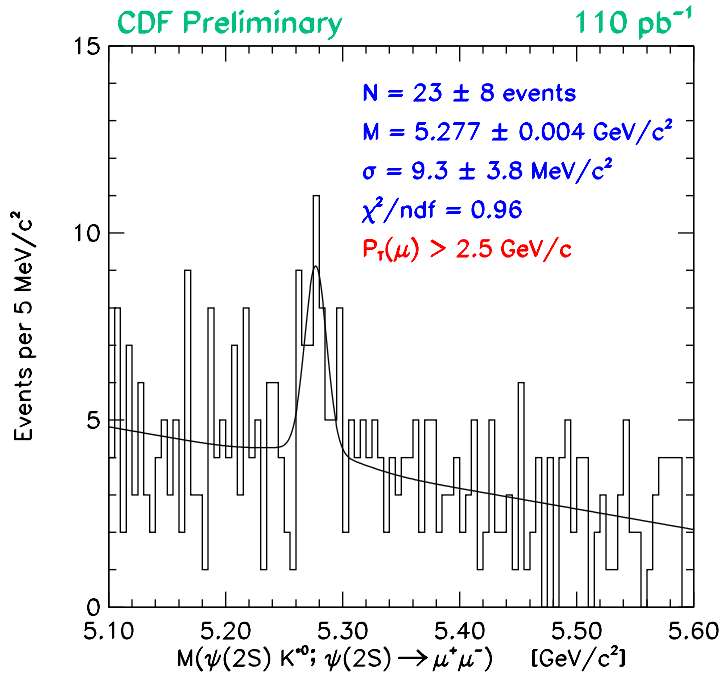


Figure 11: The  $\psi(2S)K^{*0}; \psi(2S) \rightarrow \mu^+\mu^-$  invariant mass distribution with the  $P_T(\mu^+) > 2.5$  GeV/c requirement. The fit is to a double Gaussian signal and a linear background. The first three fit parameters shown describe the Gaussian distribution of the correct  $K-\pi$  combinations.

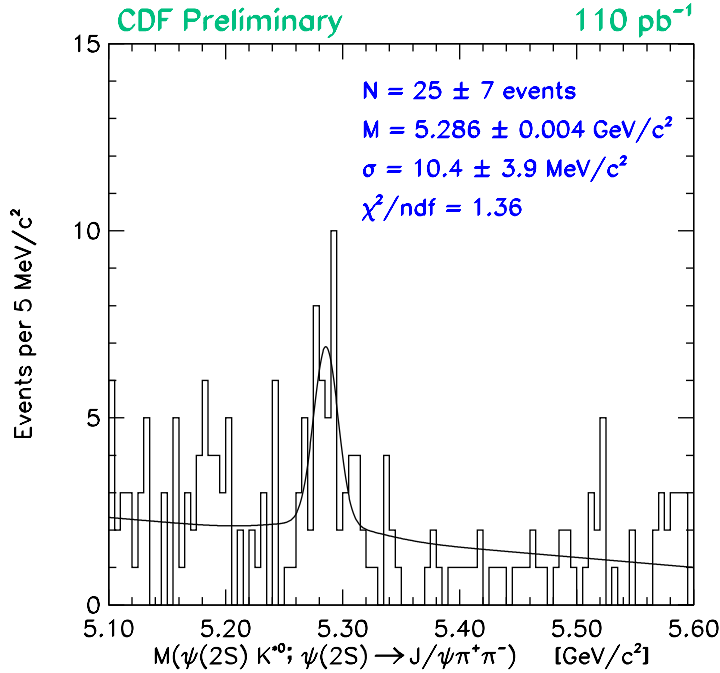


Figure 12: The  $\psi(2S)K^{*0}; \psi(2S) \rightarrow J/\psi\pi^+\pi^-$  invariant mass distribution. The fit is to a double Gaussian signal and a linear background. The first three fit parameters shown describe the Gaussian distribution of the correct  $K-\pi$  combinations.

Decay Mode	Value
$B^+ \rightarrow J/\psi K^+$	$0.02296 \pm 0.00050$
$B^+ \rightarrow \psi(2S)K^+; \psi(2S) \rightarrow \mu^+\mu^-$	$0.02474 \pm 0.00052$
$B^+ \rightarrow \psi(2S)K^+; \psi(2S) \rightarrow J/\psi\pi^+\pi^-$	$0.00747 \pm 0.00020$
$B^0 \rightarrow J/\psi K^{*0}$	$0.00777 \pm 0.00029$
$B^0 \rightarrow \psi(2S)K^{*0}; \psi(2S) \rightarrow \mu^+\mu^-$	$0.00942 \pm 0.00032$
$B^0 \rightarrow J/\psi K^{*0}$	$0.01053 \pm 0.00033$
$B^0 \rightarrow \psi(2S)K^{*0}; \psi(2S) \rightarrow J/\psi\pi^+\pi^-$	$0.00470 \pm 0.00015$

Table 2: A summary of the Monte Carlo calculated absolute geometric and kinematic acceptance for each decay mode. The grouping is on the basis of common selection criteria.

$CL(\chi^2)$ Cut Efficiency	Measurement
$\epsilon_{J/\psi}^v$	$0.967 \pm 0.010$
$\epsilon_{J/\psi}^{vm}$	$0.958 \pm 0.002$
$\epsilon_{\mu\mu}^v$	$0.932 \pm 0.019$
$\epsilon_{\mu\mu}^{vm}$	$0.940 \pm 0.017$
$\epsilon_{\pi\pi}^v$	$0.853 \pm 0.014$
$\epsilon_{\pi\pi}^{vm}$	$0.945 \pm 0.013$

Table 3: A summary of the measured  $CL(\chi^2)$  cut efficiencies;  $\epsilon^v$  denotes the  $CL(\chi^2)$  efficiency for a least-squares vertex constrained fit, and  $\epsilon^{vm}$  denotes the  $CL(\chi^2)$  efficiency for a subsequent vertex+mass constrained fit.

Table 2 contains a summary of the geometric and kinematic acceptances. The Monte Carlo generation and detector simulation was performed in a manner similar to that described in Ref [6].

Table 3 contains a summary of the  $CL(\chi^2)$  cut efficiencies. The  $\epsilon^v$  quantities were obtained by studying the effects of  $CL(\chi^2)$  cuts on the inclusive charmonium invariant mass distributions (refer to Figures 3, 4, and 5) and on the corresponding normalized ( $M/\sigma_M$ ) invariant mass distributions. The  $\epsilon^{vm}$  quantities were determined by relating the area of the fits to the normalized invariant mass distributions (with the  $CL(\chi^2) > 0.01$  vertex cut applied) in a  $\pm 2.58\sigma$  window to the entire signal fit area.

Table 4 contains the  $c\tau$  cut efficiencies in the  $B^+$  and  $B^0$  modes. In this analysis, both the numerator and denominator in each ratio of branching fractions share the same flavour of  $B$

Decay Mode	Central	$-1\sigma$	$+1\sigma$	Efficiency
$B^+ \rightarrow J/\psi K^+$	0.753	0.741	0.764	$0.753 \pm 0.012$
$B^+ \rightarrow \psi(2S)K^+; \psi(2S) \rightarrow \mu^+\mu^-$	0.738	0.726	0.748	$0.738 \pm 0.013$
$B^+ \rightarrow \psi(2S)K^+; \psi(2S) \rightarrow J/\psi\pi^+\pi^-$	0.762	0.750	0.774	$0.762 \pm 0.012$
$B^0 \rightarrow J/\psi K^{*0}$	0.755	0.742	0.766	$0.755 \pm 0.013$
$B^0 \rightarrow \psi(2S)K^{*0}; \psi(2S) \rightarrow \mu^+\mu^-$	0.749	0.736	0.760	$0.749 \pm 0.013$
$B^0 \rightarrow \psi(2S)K^{*0}; \psi(2S) \rightarrow J/\psi\pi^+\pi^-$	0.761	0.748	0.773	$0.761 \pm 0.013$

Table 4: Measured  $c\tau$  cut efficiencies in the  $B^+$  and  $B^0$  decay modes. The  $\pm 1\sigma$  efficiency variations correspond to  $\pm 1\sigma$  variations in the world average  $B^+$  and  $B^0$   $c\tau$  values.

meson; therefore, the efficiency of the  $c\tau(B) > 100 \mu\text{m}$  criterion is expected to be similar for both decay modes. The world average proper lifetime of  $B$  mesons, however, is short enough that the efficiency of a  $100 \mu\text{m}$  proper decay length cut is sensitive to the resolution of the  $c\tau$  measurement itself. Here the different decay topologies can play a measurable rôle in the efficiency, owing to the  $c\tau$  resolution dependence on the multiplicity of candidate tracks that possess SVX as well as CTC tracking information.

## 6 Summary of the Systematic Uncertainties

The systematic uncertainties associated with the generated  $B$  meson  $P_T$  spectrum are determined by varying Monte Carlo generation parameters and observing the consequent effects on the relative geometric and kinematic acceptance. A summary of the resultant systematic uncertainties is given in Table 5.

The efficiency of the global vertex  $CL(\chi^2)$  cut on the candidate  $B$  decays is expected to be similar to those calculated for the inclusive charmonium decays (refer to Table 3). Due to the fact that the bottom and strange meson species in the numerators and denominators are identical, the global  $B$   $CL(\chi^2)$  cut efficiency should cancel in the ratio. This is difficult to test in practice because the  $B$  channels do not afford the statistics that the inclusive charmonium mesons offer. To accommodate any possible non-cancellation of the global  $B$   $CL(\chi^2)$  cut efficiencies for a given ratio of branching fractions, we conservatively assign a systematic uncertainty equal to the largest  $\epsilon^v$  uncertainty from among those vertex  $CL(\chi^2)$  cuts that do not cancel in the ratio. Table 6 summarizes the global  $CL(\chi^2)$  systematic uncertainty for each ratio of branching fractions.

Efficiency Ratio	Systematic Uncertainty (%)
$\frac{B^+ \rightarrow \psi(2S)K^+; \psi(2S) \rightarrow \mu^+ \mu^-}{B^+ \rightarrow J/\psi K^+}$	$\pm 1.3$
$\frac{B^+ \rightarrow \psi(2S)K^+; \psi(2S) \rightarrow J/\psi \pi^+ \pi^-}{B^+ \rightarrow J/\psi K^+}$	$\pm 4.6$
$\frac{B^0 \rightarrow \psi(2S)K^{*0}; \psi(2S) \rightarrow \mu^+ \mu^-}{B^0 \rightarrow J/\psi K^{*0}}$	$\pm 1.0$
$\frac{B^0 \rightarrow \psi(2S)K^{*0}; \psi(2S) \rightarrow J/\psi \pi^+ \pi^-}{B^0 \rightarrow J/\psi K^{*0}}$	$\pm 1.9$

Table 5: A summary of the systematic uncertainties on the relative geometric and kinematic acceptance due to variations in the generated  $P_T$  spectrum.

Ratio of Branching Fractions	Systematic Uncertainty (%)
$\frac{B^+ \rightarrow \psi(2S)K^+; \psi(2S) \rightarrow \mu^+ \mu^-}{B^+ \rightarrow J/\psi K^+}$	$\pm 2.0$
$\frac{B^+ \rightarrow \psi(2S)K^+; \psi(2S) \rightarrow J/\psi \pi^+ \pi^-}{B^+ \rightarrow J/\psi K^+}$	$\pm 1.7$
$\frac{B^0 \rightarrow \psi(2S)K^{*0}; \psi(2S) \rightarrow \mu^+ \mu^-}{B^0 \rightarrow J/\psi K^{*0}}$	$\pm 2.0$
$\frac{B^0 \rightarrow \psi(2S)K^{*0}; \psi(2S) \rightarrow J/\psi \pi^+ \pi^-}{B^0 \rightarrow J/\psi K^{*0}}$	$\pm 1.7$

Table 6: A summary of the systematic uncertainties on the ratios of branching fractions due to the possible non-cancellation of the global vertex  $CL(\chi^2)$  cut efficiencies.

The  $PBFAC > 0.55$   $B$  candidate isolation criterion, defined in Section 3, has an efficiency that does not divide to unity in the ratio of branching fractions. Specifically, the disparity in the multiplicity of final state particles in the numerator and denominator for the  $\psi(2S) \rightarrow J/\psi\pi^+\pi^-$  ratio of branching fractions and the kinematical differences between the  $\psi(2S)$  and  $J/\psi$  states cause variations in the  $PBFAC$  isolation cut efficiency. Such variations have been measured, yielding a systematic uncertainty of 2.0% for each of the ratios of branching fractions in the analysis.

The most significant contribution to the systematic uncertainties in this study arises from the charmonium branching fractions and their associated uncertainties taken from the Particle Data Group[1]. They are:

- $\mathcal{B}(\psi(2S) \rightarrow \mu^+\mu^-) = (7.7 \pm 1.7) \times 10^{-3}$ ;
- $\mathcal{B}(\psi(2S) \rightarrow J/\psi\pi^+\pi^-) = (3.24 \pm 0.26) \times 10^{-1}$ ;
- $\mathcal{B}(J/\psi \rightarrow \mu^+\mu^-) = (5.97 \pm 0.25) \times 10^{-2}$ .

## 7 Relative Branching Fractions

The congruity between the numerators and denominators in the ratios of branching fractions furnishes several simplifications. Since the data sample is common to both modes in each ratio, the time-integrated luminosity,  $\int \mathcal{L} dt$ , divides out. The bottom meson flavours in both modes are identical, and so the  $b$  quark production cross section,  $\sigma(p\bar{p} \rightarrow b)$ , and the applicable  $b$  quark fragmentation probability,  $f_u$  or  $f_d$ , also cancel. Similarly, the like strange meson species in both the numerator and denominator mean that the ratio remains independent of the  $K^+$  and  $K^{*0}$  reconstruction efficiencies, including contributions from in-flight kaon decays. Moreover, the uniformity of the vector-pseudoscalar and vector-vector final states in each ratio permits us to ignore any polarization amplitude contributions to the acceptance.

The event yields, efficiencies, charmonium branching fractions, and systematic uncertainties are combined into the calculations of the ratios of branching fractions. The results for both the  $K^+$  and  $K^{*0}$  ratios are presented in Table 7. The  $\psi(2S) \rightarrow \mu^+\mu^-$  and  $\psi(2S) \rightarrow J/\psi\pi^+\pi^-$  contributions have been combined to produce single measurements in each case.

Ratio of Branching Fractions	Measurement
$\frac{\mathcal{B}(B^+ \rightarrow \psi(2S)K^+)}{\mathcal{B}(B^+ \rightarrow J/\psi K^+)}$	$0.666 \pm 0.093 \pm 0.101$
$\frac{\mathcal{B}(B^0 \rightarrow \psi(2S)K^{*0})}{\mathcal{B}(B^0 \rightarrow J/\psi K^{*0})}$	$0.569 \pm 0.131 \pm 0.074$

Table 7: A summary of the ratios of branching fractions, where the  $\psi(2S) \rightarrow \mu^+\mu^-$  and  $\psi(2S) \rightarrow J/\psi\pi^+\pi^-$  contributions have been consolidated. The first uncertainty is statistical and the second is systematic.

Branching Fraction	Measurement
$\mathcal{B}(B^+ \rightarrow \psi(2S)K^+)$	$(6.8 \pm 1.0 \pm 1.4) \times 10^{-4}$
$\mathcal{B}(B^0 \rightarrow \psi(2S)K^{*0})$	$(9.0 \pm 2.1 \pm 2.0) \times 10^{-4}$

Table 8: The derived absolute branching fractions, where the  $\psi(2S) \rightarrow \mu^+\mu^-$  and  $\psi(2S) \rightarrow J/\psi\pi^+\pi^-$  contributions have been consolidated. The first uncertainty is statistical and the second is systematic.

## 8 Absolute Branching Fractions

The measured ratios of branching fractions in Table 7 can be combined with the world average values for  $\mathcal{B}(B^+ \rightarrow J/\psi K^+)$  and  $\mathcal{B}(B^0 \rightarrow J/\psi K^{*0})$  to extract the absolute branching fractions  $\mathcal{B}(B^+ \rightarrow \psi(2S)K^+)$  and  $\mathcal{B}(B^0 \rightarrow \psi(2S)K^{*0})$ , respectively. We therefore use the world average branching fractions[1]:

- $\mathcal{B}(B^+ \rightarrow J/\psi K^+) = (1.02 \pm 0.14) \times 10^{-3}$ ;
- $\mathcal{B}(B^0 \rightarrow J/\psi K^{*0}) = (1.58 \pm 0.28) \times 10^{-3}$ .

The derived absolute branching fractions are listed in Table 8 and are compared to measurements and limits from the ARGUS[7], CLEO[8], and CLEO II[9] experiments in Figure 13.

## 9 Conclusion

Using the 110 pb<sup>-1</sup> Run 1 data sample, we have observed the decay modes  $B^+ \rightarrow \psi(2S)K^+$  and  $B^0 \rightarrow \psi(2S)K^{*0}$  in both the  $\psi(2S) \rightarrow \mu^+\mu^-$  and  $\psi(2S) \rightarrow J/\psi\pi^+\pi^-$  channels. We

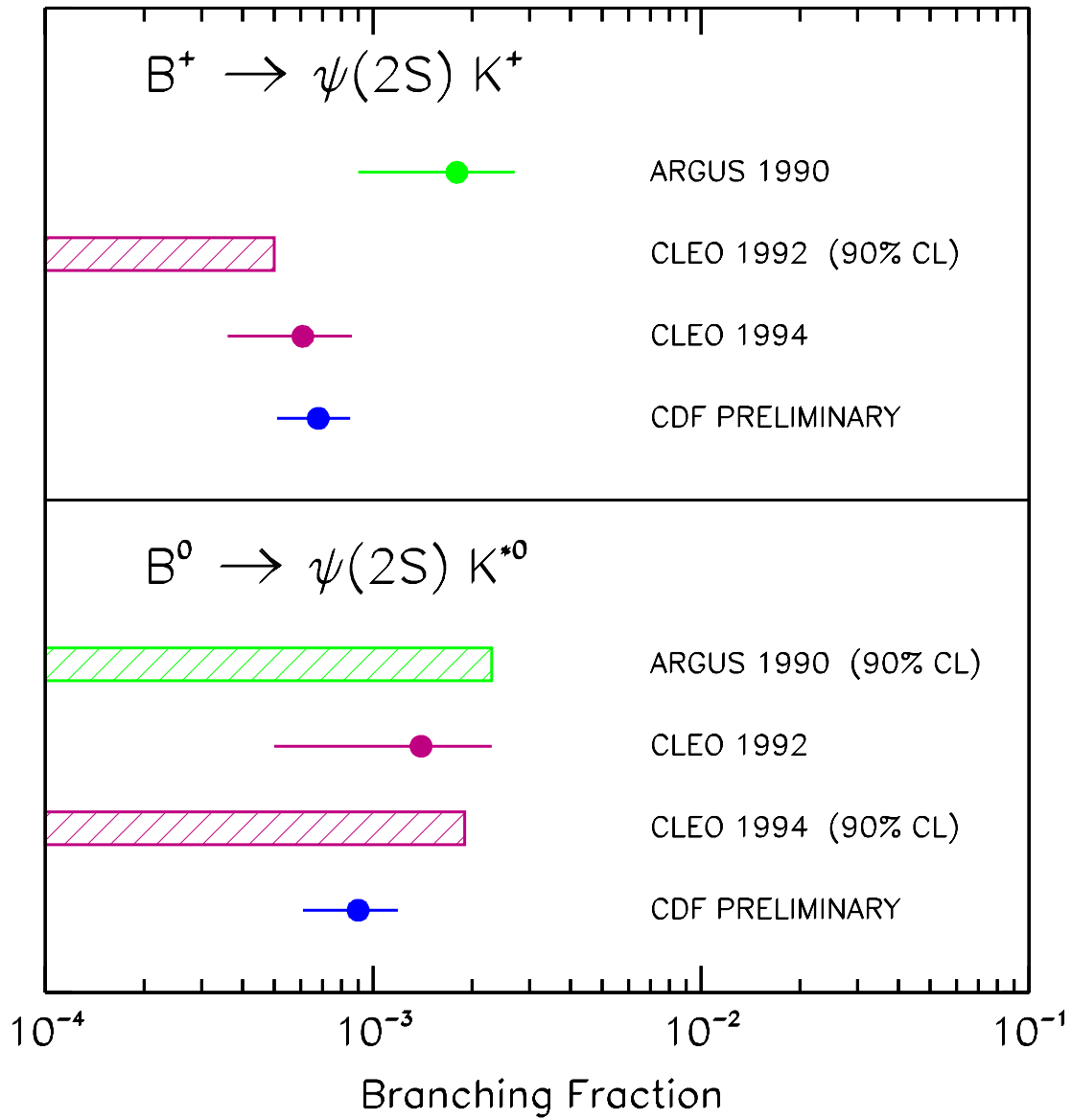


Figure 13: A comparison of the derived CDF  $B^+ \rightarrow \psi(2S)K^+$  and  $B^0 \rightarrow \psi(2S)K^{*0}$  absolute branching fractions with measurements and limits from the ARGUS, CLEO, and CLEO II experiments. The hatched bars denote 90% CL upper limits and the error bars represent the statistical and systematic uncertainties added in quadrature.

have also reconstructed the modes  $B^+ \rightarrow J/\psi K^+$  and  $B^0 \rightarrow J/\psi K^{*0}$  in order to form ratios of branching fractions with the analogous  $\psi(2S)$  decays. The measured ratios of branching fractions are summarized in Table 7. The results for the  $K^+$  and  $K^{*0}$  decay modes are consistent with one another to within the statistical uncertainties alone. We derive the absolute branching fractions  $\mathcal{B}(B^+ \rightarrow \psi(2S)K^+)$  and  $\mathcal{B}(B^0 \rightarrow \psi(2S)K^{*0})$ , shown in Table 8, and compare them with measurements and limits from other experiments (refer to Figure 13). We observe that the CDF measurements are competitive with results from other experiments.

We thank the Fermilab staff and the technical staffs of the participating institutions for their vital contributions. This work was supported by the U.S. Department of Energy and National Science Foundation; the Italian Istituto Nazionale di Fisica Nucleare; the Ministry of Education, Science and Culture of Japan; the Natural Sciences and Engineering Research Council of Canada; the National Science Council of the Republic of China; and the A. P. Sloan Foundation.

## References

- [1] Particle Data Group, L. Montanet *et al.*, Phys. Rev. D **50**, 1173 (1994).
- [2] A.N. Kamal and A.B. Santra, Phys. Rev. D **51**, 1415 (1995).
- [3] The CDF detector has a coordinate system with the  $z$  axis along the proton beam direction. The polar angle  $\theta$  is defined relative to the  $z$  axis,  $r$  is the radius from this axis, and  $\varphi$  is the azimuthal angle. Pseudorapidity is defined as  $\eta \equiv -\ln[\tan(\theta/2)]$ .
- [4] CDF Collaboration, F. Abe *et al.*, Nucl. Instrum. Methods Phys. Res. A **271**, 387 (1988); D. Amidei *et al.*, Nucl. Instrum. Methods Phys. Res. A **350**, 73 (1994); CDF Collaboration, F. Abe *et al.*, Phys. Rev. D **50**, 2966 (1994).
- [5] T.N. Pham *et al.*, Phys. Lett. **61B**, 183 (1976).
- [6] F. Abe *et al.*, FERMILAB-Pub-96/119-E, Submitted to Phys. Rev. D.
- [7] ARGUS Collaboration, H. Albrecht *et al.*, Z. Phys. C **48**, 543 (1990).
- [8] CLEO Collaboration, D. Bortoletto *et al.*, Phys. Rev. D **45**, 21 (1992).
- [9] CLEO Collaboration, M.S. Alam *et al.*, Phys. Rev. D **50**, 43 (1994).